26 February 1999

ELSEVIER

Chemical Physics Letters 301 (1999) 207–216

CHEMICAL PHYSICS LETTERS

Quantum dynamics of HF photodissociation in icosahedral $Ar_{12}HF$ clusters: rotational control of the hydrogen atom cage exit

Burkhard Schmidt *

Freie Universität Berlin, Institut für Physikalische und Theoretische Chemie, Takustrasse 3, D-14195 Berlin, Germany

Received 21 July 1998; in final form 29 December 1998

Abstract

The photodissociation dynamics of HF molecules embedded in icosahedral $HFAr_{12}$ clusters upon excitation with an ultrashort light-pulse is investigated. Assuming a frozen cluster, three-dimensional symmetry adapted wavepackets for the hydrogen photofragment are propagated in time. The emphasis is on the dependence of the HF photodissociation dynamics on the initial quantum state of the diatomic molecule. Depending on the spatial characteristics of the initial rotational state inside the rare gas cage, different cage exit probabilities are found. This opens the way to a rotational control of photochemistry of small molecules in weakly bound clusters. © 1999 Elsevier Science B.V. All rights reserved.

1. Introduction

Photochemical reactions in weakly bound van der Waals (vdW) clusters are often studied as model systems for solvation effects in chemical reaction dynamics [1,2]. Both in experiment and in theory clusters allow to investigate the stepwise growth of a 'micro-solvation' thus serving to bridge the gap between gas- and condensed-phase dynamics. The most prominent kind of solvent effects on the photochemistry of molecules is the cage effect. This notion dates back to the 1930s when a reduced quantum yield for the photolysis of iodine in solution was found [3]. Upon photo-induced breaking of a molecular bond by excitation to a repulsive state, the solvent particles may confine photofragments inside a cage formed by the solvent particles. This can lead to a delayed cage exit where photofragments undergo a few vibrational periods inside the solvent cage before they exit through the 'windows' of the cage. On a longer timescale, this confinement may also induce non-adiabatic transitions to the electronic ground state leading to re-making of the broken bond.

During the last few years, the photodissociation of hydrogen halides in a rare gas environment has emerged as a prototypical systems for the study of the solvent cage effect. For example, photodissociation in the Ar–HCl dimer has been studied by means of classical, hybrid quantum/(semi-)classical [4], approximate quantum [5], and exact quantum [5–8] simulations. The central question in all of these studies is the existence (or the extent) of the cage effect for the case of only one (or two) solvent atoms and the possible occurrence of a resonance structure in various observables. The effect of increasing solvent cluster size has been studied for photodissociation of HF in Ar_nHF ($n = 1$–54) by means of classi-

* E-mail: bschmidt@chemie.fu-berlin.de

0009-2614/99/$ - see front matter
PII: S0009-2614(99)00030-5

cal trajectories sampling a quantum initial state [9]. In another study, icosahedral $Ar_{12}HCl$ and $Ar_{54}HCl$ aggregates have been investigated in a semiclassical surface hopping study [10]. Also in matrix isolation studies hydrogen halide molecules have been established as a standard model system, see e.g. the experimental work on HCl in Ar matrices [11]. Building on earlier classical and quantum-mechanical [12] simulations of HI in Xe, semiclassical simulations of HCl in crystalline Ar have also been performed [13,14]. Moreover, quantum-mechanical simulations of the hydrogen atom wavepacket dynamics have been reported for this system [15,16].

A unique feature of photochemistry in the above-mentioned cluster and matrix systems stems from the special properties of the initial state. On the one hand, the initial solvent geometry is confined by the structure of the complex to some extent. On the other hand, there are very floppy large-amplitude motions in the electronic ground state [2]. The emphasis of the present work is on the role of the bending or rotational degrees of freedom of a hydrogen halide molecule in a rare gas cluster. For small systems with an incomplete solvation shell, the rotation is hindered by the anisotropy of the atom–molecule potentials but the amplitudes of the so-called librational motions about the equilibrium geometry can be quite extended. For larger systems with one (or more) complete solvation shells the anisotropy of the ground state interaction partly cancels and in matrices hydrogen halide molecules are known to be almost freely rotating [15,17].

In the present Letter, we want to further elucidate on the effect of the initial quantum state of the guest molecule on the photodissociation dynamics inside an icosahedral closed-shell rare gas cluster. Our main emphasis will be on the following questions: (1) What is the nature of the ground state rotational wavefunctions and how do they correlate with the cage geometry? (2) How does the cage exit probability of the hydrogen photofragment depend on the initial state and how can it be controlled by rotational pre-excitation of the molecule? For this purpose we will first calculate rotational wavefunctions in the electronic ground state and then propagate three-dimensional wavepackets in the electronically excited state to simulate the processes of caging and cage exit quantum-mechanically.

As a model system, we choose icosahedral $Ar_{12}HF$ clusters which can be considered an almost ideal model system for the following reasons. First of all, the Ar–HF potential in the ground electronic state is one of best known atom–molecule potentials, and for the excited state there are reasonably accurate data. Furthermore, it is known from matrix spectroscopy, that HF can rotate almost freely in argon and that the effect of rotation–translation coupling (RTC) can be safely neglected. Finally, for a cluster with only one shell, the photodissociation is complete on a timescale of < 100 fs so that non-adiabatic transitions and recombination play a negligible role for the short time dynamics. Details of our model and the theoretical methods are given in Section 2. The technique of symmetry adaption is described in Appendix A. The results are presented and discussed in Section 3. The final Section 4 summarizes our findings and gives conclusions.

2. Methodology

2.1. Interactions

The interactions of pure rare gases as well as of systems doped with hydrogen halide systems are among the most thoroughly studied interatomic and intermolecular forces. The electronic ground state interaction is, to a good accuracy, dominated by pairwise interactions of the closed-shell particles. Hence, the potential energy surface (PES) for $Ar_{12}HF$ is constructed as a pairwise sum of atom–molecule and atom–atom potentials similar to previous studies, see e.g. Ref. [9],

$$V_g = \sum_{i=1}^{n} V_{Ar_i,\,HF} + \sum_{i<j} V_{Ar_i,\,Ar_j}, \qquad (1)$$

where $V_{Ar_i,\,HF}$ is the anisotropic Ar–HF potential formulated in a vibrationally adiabatic representation. Its long-range part is fixed using known dispersion coefficients, the short and medium range has been determined by fitting a highly flexible model function to the best available infrared and far-infrared spectroscopic data of the Ar–HF complex [18]. The second term $V_{Ar_i,\,Ar_j}$ represents the interaction between a pair i and j of Ar atoms. We use an

Ar–Ar potential function from the literature which is based on a multi-property fit [19].

It is noted that the pairwise approach of Eq. (1) has been shown to reproduce all experimental HF vibrational frequency shifts for small clusters ($n = 1$–4) [20] evenly well as for the matrix case [17]. Including also three-body interactions causes only small corrections [21].

The potential energy surface for the electronically excited state is constructed as a sum of pairwise additive atom–atom contributions:

$$V_e = V_{HF} + \sum_{i=1}^{n} V_{Ar_i,H} + \sum_{i=1}^{n} V_{Ar_i,F} + \sum_{i<j} V_{Ar_i,Ar_j}, \tag{2}$$

where V_{HF} is the repulsive $^1\Pi$ state of the HF guest molecule adapted from ab initio data available in the literature [22]. The most crucial ingredient in calculating the cage exit dynamics is the Ar–H interaction. Here we do not rely on the (semi-)empirical potentials used in all the previous simulations of the photodissociation dynamics hydrogen halides in Ar [4,9,10] but rather use results of recent quantum-chemical ab initio MP2 calculations [23]. Finally, the rare gas–halide interaction is taken from the work of Ref. [24] where potential energy curves were fitted to differential scattering cross-sections of magnetically state-selected fluorine atoms [24]. In the present work we restrict ourselves to the ground state potential ($V_{3/2,1/2}$) of Ar–F thus neglecting the orbital dynamics of the ^{2}P state [25].

2.2. Approximations

The full quantum dynamics of a system consisting of 14 atoms such as $Ar_{12}HF$ is not exactly tractable given today's computational means. Both for the calculation of stationary ground state wavefunctions as well as for the excited state wavepacket dynamics we have to restrict our model to include only the most relevant (nuclear) degrees of freedom. Hence, the following two approximations are introduced.

(1) The rare gas atoms are assumed to be frozen ($T = 0$). This is equivalent to treating the complete system like a dimer consisting of the diatomic molecule with its six degrees of freedom and a frozen Ar solvation shell of perfect icosahedral symmetry.

(2) To further reduce the dimensionality of the problem, the center of mass of the hydrogen halide molecule is assumed to be fixed at the center of the icosahedral solvation shell.

While these are relatively poor approximations for the smallest clusters they can be justified for larger clusters with a closed solvation shell where large-amplitude motions are not accessible due to the close packing. Moreover, RTC is not expected to be very strong because the range of the rotationally averaged Ar–HF interaction [18] is slightly smaller than that of the Ar–Ar interaction [19]. In the absence of ro-vibrational spectra of $Ar_{12}HF$ clusters, supporting evidence has to come from the spectroscopy of HF in Ar matrices, which indicates that both the coupling to lattice vibrations (phonons) and RTC are indeed very weak [17].

2.3. Stationary wavefunctions

In our calculations of ground state wavefunctions we suppose that rotational and vibrational degrees of freedom of the HF molecule in the Ar cluster are decoupled because the frequency scales are very well separated. Moreover, it is known that vibrational frequencies exhibit only a very small shift with respect to the gas-phase values which is in the order of only 1% of the fundamental frequency [20,26]. Consequently, the ground state wavefunction is constructed as a product of the ground vibrational wavefunction of a Morse oscillator (with parameters taken from Ref. [22]) and a two-dimensional rotational wavefunction.

The purely rotational Hamiltonian for a rigid rotation of the guest molecule is expressed in spherical coordinates as

$$\hat{H}_g = \frac{\hat{j}^2(\theta,\phi)}{2\mu r^2} + V_g(\theta,\phi), \tag{3}$$

with $\hat{j}$ being the angular momentum and μ represents the reduced mass of the $^1H^{19}F$ system. Rotational energy levels and wavefunctions are then obtained as eigenvalues and eigenvectors of the Hamiltonian represented in a spherical harmonics basis,

$$H^{(i)}_{g,jnj'n'} = Bj(j+1)\delta_{jj'}\delta_{nn'} + V_{g,jnj'n'}, \tag{4}$$

where $B = 20.15\ \mathrm{cm}^{-1}$ is the rotational constant. The matrix elements of the (ground state) potential energy (1) are obtained as integrals over the surface of a unit sphere,

$$V_{\mathrm{g},\,jnj'n'} = \int_0^{\pi} \sin\theta\,\mathrm{d}\theta \int_0^{2\pi} \mathrm{d}\phi\, Z_{jn}^{(i)}(\theta,\phi) V_{\mathrm{g}}(\theta,\phi) \times Z_{j'n'}^{(i)}(\theta,\phi)\,. \tag{5}$$

Here (real-valued) symmetry adapted spherical harmonics (SASHs) $Z(\theta,\phi)$ have been used which transform according to an irreducible representation i of the icosahedral point group $\mathrm{I_h}$, see Appendix A.

2.4. Close-coupled wavepackets

The photodissociation dynamics is modelled by promoting the initial wavefunction onto the excited state potential of Eq. (2) which corresponds to an excitation of the HF molecule to the repulsive $^1\Pi$ state. Note that the instantaneous excitation corresponds to a laser pulse which is short compared with the timescale of the subsequent dynamics. The initial wavepacket is propagated in time subject to the excited state Hamiltonian

$$\hat{H}_{\mathrm{e}} = -\frac{\hbar^2}{2\mu}\frac{1}{r}\frac{\partial^2}{\partial r^2} r + \frac{\hat{j}^2(\theta,\phi)}{2\mu r^2} + V_{\mathrm{e}}(r,\theta,\phi)\,, \tag{6}$$

where the first two terms represent the radial and angular part of the kinetic energy of the relative HF-motion, respectively, and the third term is the potential energy surface (2) of the electronically excited state of $\mathrm{Ar}_{12}\mathrm{HF}$. In analogy to the 'close-coupled wavepacket' (CCWP) method commonly used in diatom-surface scattering theory [27], the 3-D wavefunction is expressed as a sum of products of radial (r) and angular (θ,ϕ) functions:

$$\psi^{(i)}(r,\theta,\phi;t) = \sum_{j=0}^{\infty} \sum_{n=1}^{N^{(i)}(j)} \frac{\chi_{jn}^{(i)}(r,t)}{r} Z_{jn}^{(i)}(\theta,\phi)\,, \tag{7}$$

where the time-dependence is cast into the radial functions $\chi_{jn}^{(i)}(r,t)$. Inserting ansatz (7) into the time-dependent Schrödinger equation for the Hamiltonian (6) and projection on one of the angular SASH functions yields the following set of coupled equations for the radial functions:

$$\mathrm{i}\hbar\frac{\partial}{\partial t}\chi_{jn}^{(i)}(r,t) = \left(-\frac{\hbar^2}{2\mu}\frac{\partial^2}{\partial r^2} + \frac{j(j+1)\hbar^2}{2\mu r^2}\right)\chi_{jn}^{(i)}(r,t) + \sum_{j'}\sum_{n'} V_{jnj'n'}^{(i)}(r)\,\chi_{j'n'}^{(i)}(r,t)\,, \tag{8}$$

where matrix elements of the excited state potential energy surface are defined as the integrals

$$V_{jnj'n'}^{(i)}(r) = \int_0^{\pi} \sin\theta\,\mathrm{d}\theta \int_0^{2\pi} \mathrm{d}\phi\, Z_{jn}^{(i)}(\theta,\phi) \times V_{\mathrm{e}}(r,\theta,\phi) Z_{j'n'}^{(i)}(\theta,\phi)\,. \tag{9}$$

It is noted that the use of a symmetry adapted basis $Z_{j'n'}^{(i)}$ greatly reduces the numerical effort through a decreased number $\sum_j N^{(i)}(j)$ of coupled equations to be solved. For example, within the $\mathrm{A_g}$ representation the rotational state $j = 30$ is the first one where two SASHs are found ($N^{(\mathrm{A_g})}(j) = 2$) while for all lower states either one ($N^{(\mathrm{A_g})}(j) = 1$, e.g. for $j = 0$, 6, 10, 12, 16, ...) or, more often, no SASH is found ($N^{(\mathrm{A_g})}(j) = 0$). Hence, for $j \le 30$ only 13 out of 961 functions are required. Although this ratio is less favourable for the other representations of the $\mathrm{I_h}$ group, the technique of symmetry adapted wavepackets is nonetheless very worthwhile.

Moreover, it is computationally very advantageous to evaluate the integrals (9) by expanding the potential function $V_{\mathrm{e}}(r,\theta,\phi)$ in SASHs of the totally symmetric representation $(\mathrm{A_g})$ using a direct product scheme with Gauss–Legendre integration in θ and ϕ. Typically, the summation over angular momentum states is truncated at $j = 30$ and 100×200 integration points are employed. For the electronic ground state (5) a much smaller basis set ($j \le 10$) is found to be sufficient. The resulting integrals over products of three spherical harmonics can be obtained from Clebsch–Gordan coefficients [28].

The coupled Eq. (8) are solved numerically using a Fourier collocation scheme for discretization of the radial coordinate r [29]. A grid consisting of 1024 equidistant points ranging up to 4 nm was used. The time evolution operator is approximated by expansion of the exponential in a series of (complex)

Chebychev polynomials [30]. Typically, truncation after the 100th order permits a relatively long time step of 2.5 fs.

3. Results

3.1. Ground state rotational wavefunctions

In order to understand the rotational spectroscopy of $Ar_{12}HF$, the potential energy function $V_g(\theta, \phi)$ for rotation of the HF molecule in the field of the 12 surrounding Ar atoms is considered. It turns out that the potential energy surface exhibits maxima at orientations corresponding to the C_5 axes, i.e. where the H atom is pointing towards one of the Ar atoms and minima along C_3 axes. However, the modulation between maxima and minima is only 3 cm^{-1}. In view of the atom–molecule potential of Ref. [18] which features an anisotropy of >100 cm^{-1} between the Ar–HF (-220 cm^{-1}) and the Ar–FH (-107.5 cm^{-1}) geometry, this is an astonishing result. It indicates that for the twelve Ar atoms in an icosahedral arrangement, the anisotropy of the individual interactions cancels almost completely. Note that this is not the case for HF in an Ar matrix (fcc) where the undulation of the potential energy surface for rotation in the locally octahedral environment amounts to >30 cm^{-1} [15,17]. Also for the case of HCl inside an icosahedral Ar clusters or fcc Ar matrices, the modulation depth is of the order of 30 cm^{-1} [23].

Based on this potential energy surface, rotational energy levels and wavefunctions are obtained by diagonalization of the Hamiltonian matrix (4) for the rigid rotation of an HF molecule inside the first complete solvation shell. With the undulation of the potential energy surface being considerably smaller than the rotational constant of the HF molecule, the rotational energy spectrum does not differ strongly from that of a freely rotating molecule with $E_j = Bj(j+1)$, see the energy levels indicated in Fig. 1. However, there are splittings induced by the symmetry of the cage. It can be shown by group theoretical arguments that the lowest rotational state to split under the influence of a field of icosahedral symme-

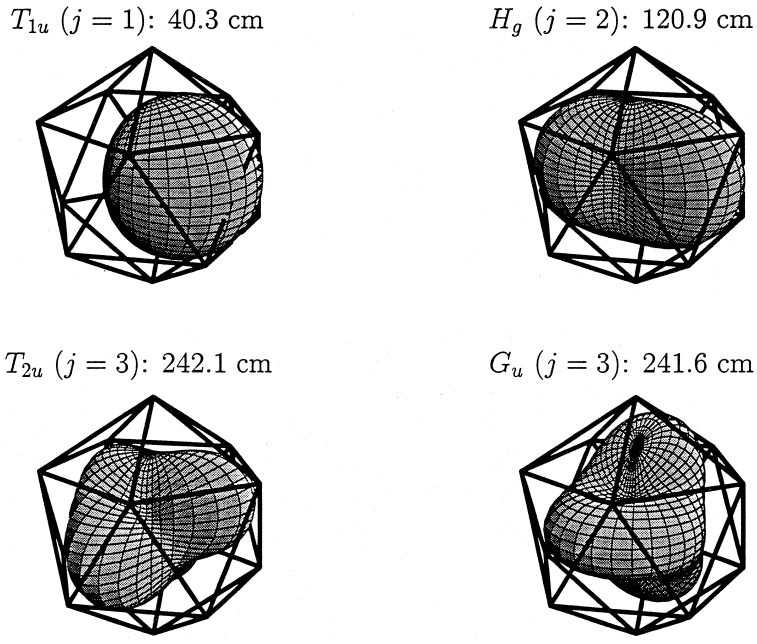

Fig. 1. Rotational wavefunctions of the HF molecule in an icosahedral $Ar_{12}HF$ cluster (electronic ground state). The angular dependence of the wavefunctions of the lowest four rotationally excited states is superimposed on a sphere. The circumscribed icosahedra illustrate the orientation relative to that of the solvent cage.

try is the $j = 3$ level. The 7-fold degeneracy is lifted and the resulting T_{2u} and G_u states are separated in energy by 0.5 cm^{-1}.

The most important consequence of the icosahedral microsolvent is the spatial characteristic of the rotational wavefunctions. The totally symmetric (A_g) rotational ground state is virtually not influenced by the icosahedral microsolvent, and it features a distribution of HF orientations which is very close to an isotropic one. Apart from the $j = 0$ state there is only a tiny admixture (5×10^{-4}) of the $j = 6$ state in the respective eigenvector. Also the first few rotationally excited states can be almost exclusively attributed to a single SASH basis function. The first two excited states $j = 1$ (T_{1u}) and $j = 2$ (H_g) exhibit preferential orientations along the C_3 axes pointing towards faces of the triangles comprising the icosahedron. Interestingly, the splitting of the $j = 3$ state results in very different rotational wavefunctions. For the T_{2u} state the extrema of the wavefunction are pointing towards corners (C_5) of the icosahedron, while the G_u state prefers the faces (C_3) and edges (C_2) but is very diffuse.

3.2. Excited state wavepacket dynamics

The wavepacket dynamics upon electronic excitation of the HF molecule is determined by the time-dependent coupled Schrödinger equations (8) for the radial functions $\chi_{jn}^{(i)}(r,t)$. In particular, the spherically averaged potential functions $V_{e,jnj'n'}^{(i)}$ are of importance. The radial dependence of the first three diagonal elements ($i = A_g$; $j = j' = 0, 6, 10$; $n = n' = 1$) are illustrated in Fig. 2. At short distances these potentials are essentially equal to the $^1\Pi$ state repulsion of the HF molecule apart from small differences caused by the centrifugal energy, see the second term on the r.h.s. of Eq. (8). At larger distances there is a barrier indicating repulsion of the hydrogen atom from the Ar solvation shell. The barrier height is strongly correlated with the angular characteristics of the corresponding SASH functions which are illustrated in the top part of Fig. 3. For the $j = 6$ state, the sharp focussing of the orientational distribution towards the Ar atoms results in a barrier that is much higher than that for the isotropic rotational ground state. In contrast, the distribution of the $j = 10$ state along C_2 and C_3 axes avoids the Ar atoms and thus

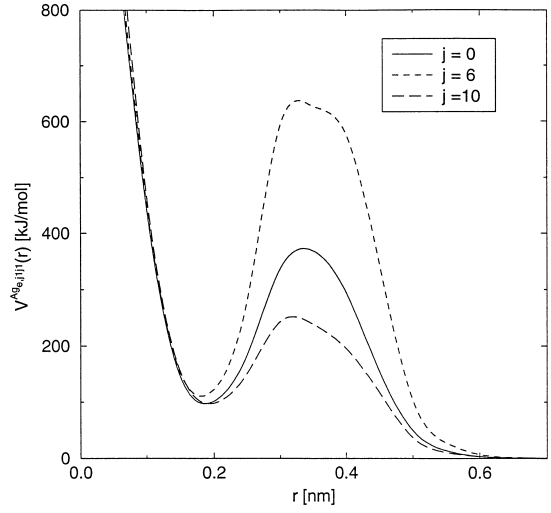

Fig. 2. Diagonal elements of the potential matrix $V_{e,j1j1}^{(A_g)}(r)$ (Eq. (9)) for the electronically excited state. The potential curves correspond to the lowest three rotational states ($j = 0, 6, 10$) which transform according to the totally symmetric irreducible representation (A_g) of the icosahedral point group I_h.

gives rise to a strongly reduced barrier. The effective potential barriers for higher rotational states are in a similar range, with the $j = 6$ and the $j = 10$ marking the extremes of strong and weak caging, respectively.

First let us consider the wavepacket dynamics for photodissociation of an HF molecule which is initially in its rotational ground state. According to the Condon approximation, we promote an initial $v = 0$, $j = 0$ product wavefunction from the electronic ground state to the electronically excited state. Initially, the expectation value of the HF distance is 94 pm which corresponds to a total energy of 509 kJ/mol on the excited state surface. Under the influence of the repulsion, the wavepacket quickly moves outwards. Approaching the potential barrier it is influenced by the non-vanishing off-diagonal elements of the potential matrix which are coupling the individual rotational states. As a consequence, higher rotational states are populated on the timescale of a few femtoseconds.

After ~ 9 fs the wavepacket has reached the top of the barrier where it undergoes bifurcation, see Fig. 3. One part of the wavepacket is reflected inwards from the cage atoms, while another part penetrates the solvent cage. The branching ratio depends on the

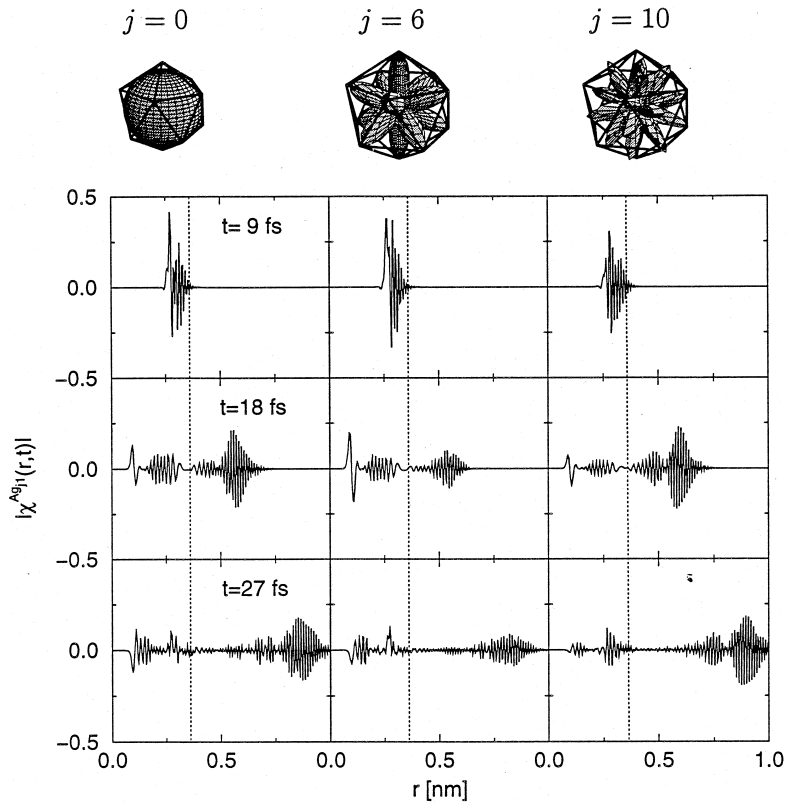

Fig. 3. Wavepacket dynamics of HCl photodissociation in a rigid icosahedral $Ar_{12}HF$ cluster. The initial state is the rotational ground state $j = 0$ (A_g). The upper part shows the first three symmetry adapted spherical harmonics (SASHs) $Z_{j1}^{(A_g)}$ for the A_g representation of the I_h point group; the lower part shows snapshots of the corresponding (time-dependent) radial wavefunctions $\chi_{j1}^{(A_g)}(r,t)$ (see Eq. (7)). The dashed horizontal lines indicate the radius of the Ar cage (0.36 nm).

rotational state. This can be seen in the snapshots for $t = 18$ fs. For $j = 6$ and $j = 10$ the probability amplitude outside the cage is smaller or larger, respectively, than for the isotropic $j = 0$ state. The reflected part undergoes quasi-bound oscillations with a period of ~ 18 fs. In the course of these oscillations, further probability amplitude is gradually leaking into the continuum of free states, see e.g. our snapshot for $t = 27$ fs.

3.3. Cage-exit probability

Analogous wavepacket propagations to simulate the photodissociation quantum dynamics of HF in $Ar_{12}HF$ are also performed for other initial state. In particular, each of the rotationally excited states of Fig. 1 ($j = 1$–3) is taken as initial states. In order to compare the results, we define the probability of cage exit as the quantum-mechanical probability to find the hydrogen photofragment after a certain time outside the solvent cage,

$$P^{(i)}(t) = \sum_{jn} \int_{r=r_c}^{\infty} |\chi_{jn}^{(i)}(r,t)|^2 , \qquad (10)$$

where r_c is a critical radius slightly larger than the cage radius beyond which there is no return of probability amplitude into the cage. We set $t = 20$ fs in order to account only for the immediate cage exit within the first vibrational period. Our findings are summarized in Fig. 4 where the cage exit probability versus the initial rotational state is shown. The first two rotationally excited states $j = 1$ (T_{1u}) and $j = 2$ (H_g) exhibit very similar cage exit probability as the rotational ground state $j = 0$ (A_g) between $P = 72\%$

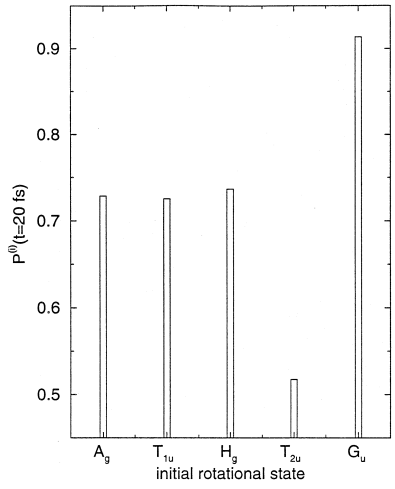

Fig. 4. Immediate cage-exit probability ($t = 20$ fs) for HF photodissociation inside an icosahedral solvation shells ($Ar_{12}HF$).

and $P = 74\%$. This indicates that the maxima of the rotational wavefunctions along a C_3 axis do not lead to an increased chance of cage exit because of the neighbouring three Ar atoms. However, the $j = 3$ states show a pronounced difference of the photodissociation dynamics. There is a strongly enhanced cage effect for the T_{2u} state ($P = 51.7\%$). In contrast, the G_u state which avoids the C_5 axes shows a much larger cage exit probability (91.3%) than any of the other states.

4. Discussion

We have studied the photodissociation of HF in icosahedral $Ar_{12}HF$ clusters. Assuming a frozen rare gas cage and a fixed HF center of mass, two sets of calculations have been performed. First, rotational states in the electronic ground state have been obtained. The most interesting finding is the T_{2u}/G_u splitting of the $j = 3$ level accompanied by different orientations of the corresponding rotational wavefunctions. Second, starting from these initial states, three-dimensional wavepackets have been propagated to model the cage exit process of the hydrogen photofragment where the use of symmetry adapted wavepackets has proved to be very instrumental. Note that two processes could be neglected that typically occur on a somewhat longer timescale ($t \geq$ 100 fs): The first one is the excitation of cage vibrations possibly leading to cage fragmentation. This assumption is justified by the relatively low energy transfer in light–heavy collisions rendering cage fragmentation relatively slow [9]. The second simplification is the restriction to purely adiabatic dynamics because: (1) the different excited states ($^1\Pi, ^3\Sigma, ^3\Pi$) are very similar to each other [22]; and (2) recombination in the ground state is slow and does not play an important role for only one solvent shell [10].

The main result of the present Letter is the strong dependence of the cage exit probability on the initial rotational state of the guest molecule inside the icosahedral cluster which is dictated by the spatial structure of the ground state rotational wavefunction. This finding opens a new way of controlling the excited state dynamics: By pre-exciting a molecule to a specific rotational state, the photodissociation quantum yield can be controlled to a certain extent. Thus the present approach represents an alternative to the recently suggested structural control by brute force alignment [31]. In particular, we have found that the cage exit dynamics upon photodissociation strongly depends on the fact whether the initial state wavefunction preferentially samples the orientations pointing towards cage atoms or pointing towards windows between them. This idea of 'rotationally mediated chemistry' has been demonstrated for the first time in Ref. [15] for matrix-isolated hydrides, in analogy to the concept of 'vibrationally mediated chemistry' already established in the 1970s [32]. In very recent work, it has been shown that the different dissociation dynamics of photofragments of librationally excited molecules can also be used to control the dynamics of subsequent reactions in weakly bound clusters [33].

Acknowledgements

The author would like to thank Professor J. Manz (FU Berlin) and Professor R.B. Gerber (HU Jerusalem and UC Irvine) for stimulating discussions. Furthermore, I am indebted to F. Neugebauer (HU Berlin) for a computer code to calculate the SASHs. Financial support by the DFG through SFB

337 ''Energy and charge transfer in molecular aggregates'' as well as a travel grant (315/PRO/ab) by a joint project of the DAAD and the NSF is acknowledged.

Appendix A. Symmetry adapted spherical harmonics (SASHs)

This appendix is concerned with the problem of obtaining symmetry adapted spherical harmonics (SASHs) $Z_{jn}^{(i)}(\theta, \phi)$ required for the expansion of the angular dependence of the wavefunctions in Eq. (7). It is noted that in the solid state literature these functions are known as surface harmonics or lattice harmonics where they are also tabulated for the point groups relevant in crystallography [34]. In contrast, SASHs for the icosahedral point group I_h have been long neglected. Stimulated by new applications of the icosahedral symmetry in chemistry (fullerenes), solid state physics (quasi-crystals), and biology (viruses), icosahedral SASHs have been investigated in recent publications, e.g. [35]. However, all of these studies are restricted to the totally symmetric irreducible representation A_g.

We employ the standard technique of forming symmetry adapted linear combinations of a set of basis functions using projection operators for a point group $\boldsymbol{G}$ consisting of $|\boldsymbol{G}|$ elements. The irreducible representations i of dimension d_i are characterized by matrix representations $\boldsymbol{D}^{(i)}(R)$ for each of the symmetry operations R. Given these representations it is straightforward to obtain SASHs $Z_{jn}^{(i)}$ by applying the projection operators $\mathbf{W}_{ts}^{(i)}$ to spherical harmonics Y_{jm},

$$Z_{jn}^{(i)} = \boldsymbol{W}_{ts}^{(i)} Y_{jm}(\theta, \phi) = \frac{d_i}{|\boldsymbol{G}|} \sum_{R \in \boldsymbol{G}} \left[D^{(i)}(R)_{ts} \right]^* R Y_{jm}(\theta, \phi), \qquad (A.1)$$

where it is sufficient to take only the diagonal elements of the representation matrices into account ($t = s$). The basis functions obtained for each of the irreducible representations have to be orthogonalized using the standard Gram–Schmidt procedure. The high symmetry of the icosahedral point group is reflected in the small number $N^{(i)}(j)$ of linearly independent SASHs.

The transformation of spherical harmonics under the various symmetry operations R in Eq. (A.1) results in a coupling of different m-sublevels of the same angular momentum j,

$$R Y_{jm}(\theta, \phi) = \sum_{n=-j}^{j} P_R \mathscr{D}_{jnm}(\alpha, \beta, \gamma) Y_{jn}(\theta, \phi). \qquad (A.2)$$

In case of a proper rotation α, β, γ are the Euler angles corresponding to the symmetry operation R and the factor P_R is unity. Improper rotations can be regarded as a product of a proper rotation about the above Euler angles and an inversion where $P_R = (-1)^j$ applies. Expressions for the evaluation of the Wigner coefficients $\mathscr{D}_{jnm}$ can be found in Ref. [28]:

$$\mathscr{D}_{jnm}(\alpha, \beta, \gamma) = \begin{cases} \exp[-\mathrm{i}m(\alpha+\gamma)]\delta_{n,m} & \text{for } \beta = 0, \\ (-1)^j \exp[-\mathrm{i}m(\alpha-\gamma)]\delta_{n,-m} & \text{for } \beta = \pi, \\ (-1)^l \exp[-\mathrm{i}(m\alpha+n\gamma)] d_{jnm}(\beta) & \text{else}, \end{cases} \qquad (A.3)$$

with $l = |n| + n - |m| - m$. The β-dependent reduced matrices are given by

$$d_{jnm}(\beta) = \sum_{k=\max(0, m-n)}^{\min(j-n, j+m)} (-1)^k \times \frac{\sqrt{(j+n)!(j+m)!(j-n)!(j-m)!}}{(j-n-k)!(j+m-k)!k!(k-m+n)!} \times [\cos(\beta/2)]^{2j+m-n-2k} \times [\sin(\beta/2)]^{2k+n-m}. \qquad (A.4)$$

The coefficients $d_{jnm}(\beta)$ of Eq. (A.4) are calculated numerically using a recursion relation given in Ref. [34]. In the present work, SASHs for each of the 10 irreducible representations of the I_h point group have been calculated for $j \leq 45$ using Eq. (A.1). The tabulated coefficients are available from the author on request.

References

[1] C. Wittig, S. Sharpe, R.A. Beaudet, Acc. Chem. Res. 21 (1988) 341.
[2] R.B. Gerber, A.B. McCoy, A. Garcia-Vela, Annu. Rev. Phys. Chem. 45 (1994) 275.

[3] J. Franck, E. Rabinovitch, Trans. Faraday Soc. 30 (1934) 120.
[4] A. Garcia-Vela, R.B. Gerber, J. Chem. Phys. 98 (1993) 427.
[5] T. Schröder, R. Schinke, M. Mandziuk, Z. Bačić, J. Chem. Phys. 100 (1994) 7239.
[6] T. Schröder, R. Schinke, Z. Bačić, Chem. Phys. Lett. 235 (1995) 316.
[7] A. Garcia-Vela, R.B. Gerber, J. Chem. Phys. 103 (1995) 3463.
[8] E. Narevicius, N. Moiseyev, Chem. Phys. Lett. 287 (1998) 250.
[9] T. Schröder, R. Schinke, S. Liu, Z. Bačić, J.W. Moskowitz, J. Chem. Phys. 103 (1995) 9228.
[10] M.Y. Niv, A.I. Krylov, R.B. Gerber, Faraday Discuss. 108 (1998) 243.
[11] K.H. Gödderz, N. Schwentner, M. Chergui, J. Chem. Phys. 105 (1996) 451.
[12] R. Alimi, R.B. Gerber, Chem. Phys. Lett. 173 (1990) 393.
[13] I.H. Gersonde, H. Gabriel, J. Chem. Phys. 98 (1993) 2094.
[14] A.I. Krylov, R.B. Gerber, J. Chem. Phys. 106 (1997) 6574.
[15] J. Manz, P. Saalfrank, B. Schmidt, J. Chem. Soc., Faraday Trans. 93 (1997) 957, see also http://www.rsc.org/is/journals/clic_rsc/net_4.htm.
[16] F. Neugebauer, V. May, Chem. Phys. Lett. 289 (1998) 67.
[17] D.T. Anderson, J.S. Winn, Chem. Phys. 189 (1994) 171.
[18] J.M. Hutson, J. Chem. Phys. 96 (1992) 6752.
[19] R.A. Aziz, H.H. Chen, J. Chem. Phys. 67 (1977) 5719.
[20] Z. Bacic, J. Chem. Soc., Faraday Trans. 93 (1997) 1459.
[21] M. Lewerenz, J. Chem. Phys. 104 (1996) 1028.
[22] T.H. Dunning Jr., J. Chem. Phys. 65 (1976) 3854.
[23] P. Žďánská, B. Schmidt, P. Jungwirth, J. Chem. Phys. (in press).
[24] E. Aquilanti, E. Luzzatti, F. Pirani, G.G. Volpi, J. Chem. Phys. 89 (1988) 6165.
[25] A.I. Krylov, R.B. Gerber, V.A. Apkarian, Chem. Phys. 189 (1994) 261.
[26] B. Schmidt, P. Jungwirth, Chem. Phys. Lett. 259 (1996) 62.
[27] D.J. Kouri, R.C. Mowrey, J. Chem. Phys. 86 (1987) 2087.
[28] R.N. Zare, Angular Momentum, Wiley, New York, 1987.
[29] R. Kosloff, Annu. Rev. Phys. Chem. 45 (1994) 145.
[30] H. Tal-Ezer, R. Kosloff, J. Chem. Phys. 81 (1984) 3967.
[31] R.J. Hinde, Chem. Phys. Lett. 283 (1998) 125.
[32] V.S. Letokhov, Science 180 (1973) 451.
[33] P. Jungwirth, P. Žďánská, B. Schmidt, J. Phys. Chem. 102 (1998) 7241.
[34] C.J. Bradley, A.P. Cracknell, The Mathematical Theory of Symmetry in Solids, Clarendon, Oxford, 1972.
[35] W. Prandl, P. Schiebel, K. Wulf, Acta Crystallogr. A 52 (1996) 171.